Crystal structure of oxygen-evolving photosystem II at 1.9 Å resolution

Yasufumi Umena[1, †, *], Keisuke Kawakami[2, ‡, *], Jian-Ren Shen[2, §], Nobuo Kamiya[1, ¶, §],

[1]Department of Chemistry, Graduate School of Science, Osaka City University, 3-3-138 Sugimoto, Sumiyoshi, Osaka 558-8585, Japan; [2]Division of Bioscience, Graduate School of Natural Science and Technology/Faculty of Science; Okayama University, Okayama 700-8530; Japan.

[†]Present address: Institute for Protein Research, Osaka University, Suita, Osaka, Japan.
[‡]Present address: Department of Chemistry, Graduate School of Science, Osaka City University, 3-3-138 Sugimoto, Sumiyoshi, Osaka 558-8585, Japan
[¶]Present address: The OCU Advanced Research Institute for Natural Science and Technology (OCARINA), Osaka City University, 3-3-138 Sugimoto, Sumiyoshi, Osaka 558-8585, Japan

*These authors contributed equally to this work.

[§]Corresponding authors: shen@cc.okayama-u.ac.jp; nkamiya@sci.osaka-cu.ac.jp

Summary

Photosystem II is the site of photosynthetic water oxidation, and contains 20 subunits with a total molecular mass of 350 kDa. The structure of photosystem II has been reported at 3.8 to 2 .9 Å resolutions. Here we report the crystal structure of photosystem II at 1.9 Å resolution. From our electron density map, we located all of the metal atoms of the Mn_4CaO_5-cluster, together with all of their ligands. We found that 5 oxygen atoms served as oxo-bridges linking the 5 metal atoms, and 4 water molecules were bound to the Mn_4CaO_5-cluster; some of them may therefore serve as substrates for di-oxygen formation. We identified more than 1300 water molecules in a photosystem II monomer, some of them formed extensive hydrogen-bonding networks that may serve as channels for protons, water or oxygen molecules. The determination of the high resolution structure of photosystem II will allow us to analyze and understand its functions in a great detail.

Photosystem II (PSII) is a membrane-protein complex located in the thylakoid membranes of oxygenic photosynthetic organisms, and performs a series of light-induced electron transfer reactions leading to the splitting of water into protons and molecular oxygen. The products of PSII, namely, chemical energy and oxygen, are indispensable for sustaining life on the earth. PSII from cyanobacteria is composed of 17 trans-membrane subunits and 3 peripheral proteins, a number of cofactors, with a total molecular weight of 350 kDa. The light-induced water oxidation is catalyzed by a Mn_4Ca-cluster composed of 4 Mn atoms and 1 Ca atom, which cycles through several different Si-states (with i=0-4) upon extraction of each electron by the PSII reaction center (PSII-RC) P_{680}[1, 2]. When 4 electrons and 4 protons are extracted from 2 molecules of water, 1 molecule of di-oxygen is formed. The structure of PSII has been solved at 3.8-2.9 Å resolutions from two closely related thermophilic cyanobacteria, *Thermosynechococcus elongatus*[3-5] and *T. vulcanus*[6]. These structural studies provided the arrangement of all of the protein subunits, the locations of chlorophylls as well as other cofactors, and formed a basis for further investigations on the functions of PSII. However, the resolution achieved so far was not high enough to unravel the structure of the Mn_4Ca-cluster, the location of substrate water molecules, as well as the precise arrangement of the amino acid side chains and cofactors that may have significant mechanistic consequences to the energy, electron, and proton transfer reactions. We have improved the resolution of the PSII crystals from *T. vulcanus* to 1.9 Å, and analyzed its structure. Here we present the crystal structure of oxygen-evolving PSII at 1.9 Å resolution, which provided much more details on the arrangement, coordination environments of the Mn_4Ca-cluster as well as other cofactors and water molecules.

Overall structure

The structure of PSII dimer was analyzed at 1.9 Å resolution (Methods and Supplementary Figure 1, Table 1), and the overall structure was shown in Fig. 1. Every PSII monomer contained 19 protein subunits, among which, PsbY was not found, suggesting that this subunit has been lost during purification or crystallization, presumably due to its loose association with PSII[4-6, 7, 8)]. The C_α superposition of our PSII dimer with the structure reported at 2.9 Å resolution[5] yielded a r.m.s. value of 0.78 Å, indicating that the overall structure determined at 2.9 Å resolution is well preserved in our present structure.

In addition to the protein subunits, 35 chlorophylls, 2 pheophytins, 11 β-carotenes, more than 20 lipids, 2 plastoquinones, 2 heme irons, 1 non-heme iron, 4 Mn atoms, 3-4 Ca atoms (among which, 1 is in the Mn_4Ca-cluster), 3 Cl^- ions (among which, 2 are in

the vicinity of the Mn_4Ca-cluster), 1 bicarbonate ion, and more than 15 detergents were found (Supplementary Table 2). Within each PSII monomer, more than 1300 water molecules were found, yielding a total of 2795 water molecules in a dimer (Fig. 1a) (Supplementary Table 1). As shown in Fig. 1b, the water molecules were organized into two layers located on the surfaces of the stromal and lumenal sides, respectively, with the latter having more water molecules than the former. A few water molecules were found within the membrane region, most of them served as ligands to chlorophylls (see below). In the following we describe the detailed structure and functions of the Mn_4CaO_5-cluster as well as other cofactors based mainly on the structure of monomer A (labeled with capital letters). There were some slight differences in the structures between two monomers within a dimer; however, most of them are not related with the critical functions of PSII.

Structure of the Mn_4CaO_5-cluster

The electron densities for 4 Mn atoms and 1 Ca atom in the oxygen-evolving complex (OEC) were well defined and clearly resolved, and the electron density for the Ca atom was lower than those of the 4 Mn atoms, allowing us to assign the individual Mn and Ca atoms unambiguously (Fig. 2a)[4, 5]. In addition, 5 oxygen atoms were found to serve as oxo-bridges linking the 5 metal atoms from the omit map (Fig. 2a). This gives rise to a Mn_4CaO_5-cluster. Among these 5 metals and 5 oxygen atoms, 3 Mn, Ca, and 4 oxygen atoms form a cubane-like structure in which, the Ca atom and 3 Mn atoms occupy four corners and 4 oxygen atoms constitute the other four corners. The bond lengths between oxygen and Ca atom within the cubane are generally in the range of 2.4-2.5 Å, and those between oxygen and Mn atoms are in the range of 1.8-2.1 Å (Fig. 2b). However, the bond distance between one of the oxygen atoms at the corner of the cubane (O5) and Ca is 2.7 Å, and those between O5 and Mn atoms are in the range of 2.4-2.6 Å. Due to these differences in the bond lengths, the Mn_3CaO_4-cubane is not an ideal, symmetric one.

The fourth Mn (Mn4) is located outside of the cubane, and is linked to two Mn atoms (Mn1 and Mn3) within the cubane by O5 and the fifth oxygen atom (O4) via a di-μ-oxo-bridge. In this way, every two adjacent Mn atoms are linked by di-μ-oxo-bridges; namely, Mn1 and Mn2 are linked by a di-μ-oxo-bridge via O1 and O3, Mn2 and Mn3 are linked via O2 and O3, and Mn3 and Mn4 are linked via O4 and O5. On the other hand, Ca is linked to all 4 Mn atoms by oxo-bridges, namely, to Mn1 via the di-μ-oxo-bridge formed by O1 and O5, to Mn2 via O1 and O2, to Mn3 via O2 and O5, and to Mn4 via the mono-μ-oxo-bridge by O5. The whole structure of the Mn_4CaO_5

cluster resembles a distorted chair, with the distorted cubane serving as the seat base and the isolated Mn4 and O4 serving as the back of the chair. The cubane-like structure has been reported previously[4, 9-12], but the oxo-bridges and exact distances among the individual atoms could not be determined at the medium resolution[4].

The distances among the 4 Mn atoms determined for monomer A are: Mn1-Mn2, 2.8 Å, Mn2-Mn3, 2.9 Å, Mn3-Mn4, 3.0 Å (2.9 Å for monomer B), Mn1-Mn3, 3.3 Å, Mn1-Mn4, 5.0 Å (Fig. 2c). The distances between Ca and the 4 Mn atoms are: Ca-Mn1, 3.5 Å, Ca-Mn2, 3.3 Å, Ca-Mn3, 3.4 Å, and Ca-Mn4, 3.8 Å (Fig. 2d) (for the corresponding distances of monomer B and the average distances between the two monomers, see Supplementary Table 3). These distances are largely different from those reported in the previous crystal structures[3-6], however, they are comparable with those reported from EXAFS studies[13,14] if we consider that there is an error of 0.16 Å for the distances determined from the X-ray structural analysis (Methods).

In addition to the 5 oxygen atoms, 4 water molecules (W1 to W4) were found to be associated with the Mn_4CaO_5-cluster, among which, W1 and W2 are coordinated to Mn4 with distances of 2.1 and 2.2 Å, and W3 and W4 are coordinated to Ca with a similar distance of 2.4 Å. No other water molecules were found to associate with the other 3 Mn atoms, suggesting that some of the 4 water molecules may serve as the substrates for water-oxidation.

All of the amino acid residues coordinated to the Mn_4CaO_5-cluster were identified (Fig. 2e and Supplementary Table 4), among which, D1-Glu189 served as a monodentate ligand to Mn1, which is different from the previous report showing that it serves as a bidentate ligand[5]. All of the remaining 5 carboxylate residues served as bidentate ligands, namely, D1-Asp170 as a bidentate ligand to Mn4 and Ca, D1-Glu333 to Mn3 and Mn4, D1-Asp342 to Mn1 and Mn2, D1-Ala344 (the C-terminal residue of D1) to Mn2 and Ca, and CP43-Glu354 to Mn2 and Mn3. In addition, D1-His332 is coordinated to Mn1, whereas D1-His337 is not directly coordinated to the metal cluster. Most of the distances of the ligands to Mn atoms are in the range of 2.0-2.3 Å, with two shortest distances between D1-Glu189 and Mn1 at 1.8 Å, and that between D1-Ala344 and Mn2 at 1.9 Å (Supplementary Table 3). The distances of two carboxylate ligands, D1-Asp170 and D1-Ala344 to Ca are slightly longer (2.3-2.4 Å) than the ligand distances to Mn (Supplementary Table 3). Combining with the oxo-bridges and water molecules, these gave rise to a saturating ligand environment for the Mn_4CaO_5-cluster, namely, each of the 4 Mn atoms has 6 ligands, whereas the Ca atom has 7 ligands (Supplementary Table 4). The ligation pattern and the geometric positions of the metal

atoms revealed in the present structure may have important consequences on the mechanisms of water splitting and O-O bond formation.

In addition to the direct ligands of the Mn_4CaO_5-cluster, D1-Asp61, D1-His337, and CP43-Arg357 were found to be located in the second coordination sphere and may play important roles in maintaining the structure of the metal cluster, in agreement with various reports showing the importance of these 3 residues in maintaining the oxygen-evolving activity[15-19]. One of the guanidinium η-nitrogens of CP43-Arg357 was hydrogen-bonded to both O2 and O4 of the Mn_4CaO_5-cluster, whereas the other one was hydrogen-bonded to the carboxylate oxygen of both D1-Asp170 and D1-Ala344. The imidazole □-nitrogen of D1-His337 was hydrogen-bonded to O3. These two residues may thus function to stabilize the cubane structure of the metal cluster as well as to provide partial positive charges to compensate for the negative charges brought about by the oxo-bridges and carboxylate ligands of the metal cluster. The carboxylate oxygen of D1-Asp61 is hydrogen-bonded to W1, and also to O4 indirectly through another water molecule, suggesting that this residue may also contribute to stabilizing the metal cluster. Furthermore, D1-Asp61 is located in the entrance of a proposed proton exit channel involving Cl-1 (see below), suggesting that this residue may function in facilitating proton exit from the Mn_4CaO_5 cluster[5, 20, 21].

The most significant structural feature of the Mn_4CaO_5 cluster, which may be important for elucidating the mechanism of the water-splitting reaction, is its distorted chair form. The large distortion is principally caused by the existence of Ca and O5 in the Mn_4CaO_5-cluster as described above. The apparently longer distances between O5 and metal atoms suggested that the bonds of O5 to metal atoms are weak, and therefore O5 may have a lower negative charge compared with a valence of -2 expected for normal oxygen atoms in oxo-bridges. This in turn suggests that O5 may exist as a hydroxide ion in the S_1-state, and may provide one of the substrates for the di-oxygen formation. Since both W2 and W3 are within the hydrogen-bond distances to O5, one of these two water molecules may provide another substrate.

Because the transition of S_0-to-S_1 is fastest within the Kok cycle, the proton released during S_0-to-S_1 transition may be accepted by D1-Tyr161 (also termed Y_Z) which is deprotonated via proton-coupled electron transfer (PCET, see below). W3 is closer to Y_Z than O5 (Fig. 3a), and may be a more favorable candidate than O5 as the proton releasing group. Thus, W3, instead of O5, may be a hydroxide ion in the S_1-state, which suggest that O-O bond formation may occur between W2 and W3. In any events, our results suggested that the O-O bond formation occurs within 2 of the 3 species O5, W2, W3.

Hydrogen-bond network around Y_Z

Y_Z (D1-Tyr161) is located between the Mn_4CaO_5-cluster and PSII-RC, and functions to mediate electron transfer between the Mn_4CaO_5-cluster and PSII-RC. An extensive hydrogen-bonding network was found between D1-Tyr161 and the Mn_4CaO_5-cluster, and from D1-Tyr161 to the lumenal bulk phase. D1-Tyr161 was hydrogen-bonded to the two water molecules coordinated to Ca either directly (W4) or indirectly (W3) through another water (Fig. 3a). The hydrogen-bond between the additional water and D1-Tyr161 that mediates the link from W3 to Tyr161 has a length of 2.6 Å, suggesting that this is a strong (low barrier) hydrogen-bond[22]. This additional water also mediates the hydrogen-bond between the two water molecules bound to Mn4 and D1-Tyr161. On the other hand, another strong hydrogen bond was found between D1-Tyr161 and the □-nitrogen of D1-His190, which has a distance of 2.5 Å and is in the opposite side of the Mn_4CaO_5-cluster. D1-His190 was further hydrogen-bonded to D1-Asn298 and to several water molecules and amino acid residues including CP43-Ala411, D1-Asn322, and PsbV-Tyr137, leading to an exit pathway to the lumenal bulk solution (PsbV-Tyr137 is the C-terminal residue of the PsbV subunit) (Fig. 3b). This hydrogen-bond network is located in the interfaces between D1, CP43, and PsbV subunits, and may function as an exit channel for protons that arise from proton-coupled electron transfer (PCET) via Y_Z. This is in support of the existence of a PCET pathway involving D1-Tyr161 and D1-His190 as implicated from a number of previous studies[23-25]. PsbV-Tyr137 at the exit of this channel is surrounded by several charged residues including D1-Arg323, D1-His304 and PsbV-Lys129; these residues may therefore function to regulate the proton excretion through the PCET pathway (Fig. 3b).

The other redox active tyrosine residue Y_D (D2-Tyr160) has a different, rather hydrophobic environment compared with that of Y_Z. For a discussion of the environment of Y_D, see Supplementary Fig. 3 and discussions.

The structure and function of chloride-binding sites

Previous studies have identified two chloride ions (Cl^-) in the vicinity of the Mn_4CaO_5-cluster by substitution of Cl^- by Br^- or I^- [26, 27], although only one Cl^--site was visible in the native PSII crystals[5]. In our present study, the electron density for the two Cl^--binding sites were clearly visible (Fig. 4a), which were confirmed from the anomalous diffraction Fourier map calculated with data collected at 1.75 Å wavelength (Fig. 4a). The two Cl^--binding sites are located in the same position as those reported for Br^-- or I^--substituted PSII previously[26, 27] (Fig. 4b and c). Both Cl^- ions are surrounded by four species, among which, two are water molecules. The other two species for Cl^--1

are the amino group of D2-Lys317 and the backbone nitrogen of D1-Glu333, and those for Cl^--2 are the backbone nitrogens of D1-Asn338 and CP43-Glu354. Since the side chain of D1-Glu333 and CP43-Glu354 are coordinated to the Mn_4CaO_5-cluster directly, the two Cl^- anions may function to maintain the coordination environment of the Mn_4CaO_5-cluster, thereby keeping the oxygen-evolving reaction to proceed properly.

In addition to the structural roles, the two Cl^--binding sites were found to be in the entrance of hydrogen-bond networks starting from the Mn_4CaO_5-cluster toward the lumenal bulk solution (Fig. 4b and c). The network through Cl^--1 was located in the interface between D1, D2, and PsbO subunits, and that through Cl^--2 was located in the interface of D1, CP43, and PsbU subunits. These hydrogen-bond networks involve a number of bound water molecules and some hydrophilic or charged amino acid residues; they thus may function as either proton exit channels or water inlet channels.

Chlorophylls and β-carotenes

The positions and orientations of most chlorophylls are similar to those reported previously[4-6]. However, we determined the ligands to the central Mg of all of chlorophylls, among which, 7 are coordinated by water instead of amino acid residues (Fig. 5a, Supplementary Table 5). These are Chl-6 (the accessory chlorophyll of D1), Chl-7 (the accessory chlorophyll of D2), Chl-12, Chl-18, Chl-21 harbored by CP47, and Chl-31, Chl-34 harbored by CP43. In addition, Chl-38 was coordinated by CP43-Asn39, and all other chlorophylls are coordinated by histidines. From our electron density map, we confirmed that all of the C8 and C13 positions in the phytol chains have a *R, R*-configuration, in agreement with the stereo-chemistry determined for the complete phytol chain[28,29]. Furthermore, we found that most of the vinyl groups are located in the same or near the same plane of the tetrapyrrole ring, which may contribute to the extension of energy coupling within the plane and hence facilitate the energy migration between adjacent chlorophylls.

The 4 chlorophylls constituting PSII-RC are depicted in Fig. 5b. The non-crystallographic two-fold symmetry expected for the chlorophyll dimer P_{D1} and P_{D2} is apparently broken in our high resolution structure in terms of the following aspects. The vinyl group of P_{D1} is rather in plane, and its terminal carbon atom is close to Mg of P_{D2} at its 6th coordination site. In contrast, the corresponding vinyl group of P_{D2} is out of the chlorin plane, and is located distantly from the Mg atom of P_{D1}. The edge-to-edge distances that are able to form π-π stacking or CH-π stacking among the 4 chlorophylls range from 3.3-3.5 Å, with the closest distance being 3.3 Å between P_{D1} and Chl_{D1}. This may account partly for the preferential electron transfer along the D1-side. Importantly,

although both water ligands to the two "accessory chlorophylls" Chl_{D1} and Chl_{D2} are hydrogen-bonded to the carbonyl oxygen of methoxycarbonyl group of chlorin ring V, the water ligand of Chl_{D1} was further hydrogen-bonded to D1-Thr179, whereas no such a hydrogen-bond partner was found for Chl_{D2} (Fig. 5c and d). These may also contribute to the functional differences between the two chlorophylls.

CP47 and CP43 bind 16 and 13 antenna chlorophylls, respectively, which are arranged as double layers connected by a special chlorophyll at the middle of the two layers[30]. The chlorophylls are distributed in one of three areas separated by coiled-coil helix dimers (I, II), (III, IV), and (V, VI) of CP47 (or CP43) (Fig. 5a, Supplementary Fig. 4 and discussions). A significant feature found in the present structure is that the chlorin ring of most chlorophylls are not planar, which may affect the electronic, spectroscopic, or energetic properties of the chlorophylls.

The positions and orientations of most β-carotenes (BCR) are similar to those in the previous structures (Supplementary Fig. 5 and discussions). All of the 11 β-carotenes were found to be in an all-trans type.

Plastoquinones, non-heme iron, and lipids

Q_A and Q_B were found in the positions similar to those reported previously (Supplementary Fig. 5), with Q_B being less defined and having a higher B-factor than that of Q_A. Q_C, the third quinone found in the previous structure[5], was not found in the present structure, probably due to the differences in preparation or crystallization conditions employed between the previous and present studies.

Six monogalactosyl-diacylglycerol (MGDG), 5 digalactosyl-diacylglycerol (DGDG), 4 sulfoquinovosyl-diacylglycerol (SQDG), and 5 phosphatidyl-glycerol (PG) molecules were found (Supplementary Fig. 5 and discussions). All of the SQDG and PG molecules were distributed in the stromal side, with their head groups located in the stromal surface of the membrane, whereas all of the MGDG and DGDG molecules, except one MGDG, were located in the lumenal side. These may suggest that the hydrophilic head groups of SQDG and PG cannot penetrate through the membrane, resulting in their preferential distribution in the stromal side, whereas the more hydrophobic lipids MGDG and DGDG were able to transfer across the membrane.

In conclusion, the high resolution structure of PSII revealed the geometric arrangement of the Mn_4CaO_5-cluster as well as its oxo-bridges and ligands, and 4 bound water molecules. This provided the basis for unraveling the mechanism of water-splitting and O-O bond formation, one of nature's most fascinating and important

reactions. In addition, the precise arrangement of amino acid side chains and cofactors were determined, enabling an understanding of the energy migration, electron transfer, and water-splitting reactions taken place within PSII on a solid structural basis.

METHODS SUMMARY

PSII core complexes highly active in oxygen evolution were purified from a thermophilic cyanobacterium *Thermosynechococcus vulcanus*[31, 32]. The homogeneity of PSII was improved by introducing a re-crystallization step. The previous crystallization conditions[6, 32] were improved to give rise to the high resolution crystals (Methods). A typical diffraction pattern was shown in Supplementary Fig. 1, from which diffraction spots beyond 1.8 Å resolution could be observed. In order to suppress the possible radiation damage to a minimum level, we used a slide-oscillation method, resulting in an X-ray dose on each point of the crystal to a low level compared to the previous ones[33]. A full data set was collected at a wavelength of 0.9 Å and processed to 1.9 Å resolution (Supplementary Table 1). For identifying the positions of Cl^- ions, another data set was taken at a 1.75 Å wavelength, and processed to 2.5 Å resolution.

The structure of PSII was solved by the molecular replacement method using the structure reported at 2.9 Å resolution as the search model (PDB_ID: 3BZ1)[5], and refined to R_{cryst}/R_{free} values of 0.174/0.201 with the Cruickshank's diffraction-component precision index (DPI)[34] of 0.11 Å. Detailed procedures for crystallization and structure determination can be found in Methods.

1. Kok, B., Forbush, B. & McGloin, M. Cooperation of charges in photosynthetic oxygen evolution. I. A linear four step mechanism. *Photochem. Photobiol.* **11,** 457-475 (1970).
2. Joliot, P. Period-four oscillations of the flash-induced oxygen formation in photosynthesis. *Photosynth. Res*. **76,** 65-72 (2003).
3. Zouni, A. et al. Crystal structure of photosystem II from *Synechococcus elongatus* at 3.8 Å resolution. *Nature* **409,** 739-743 (2001).
4. Ferreira, K. N., Iverson, T. M., Maghlaoui, K., Barber, J. & Iwata, S. Architecture of the photosynthetic oxygen-evolving center. *Science* **303,** 1831-1838 (2004).
5. Guskov, A., Kern, J., Gabdulkhakov, A., Broser, M., Zouni, A. & Saenger, W. Cyanobacterial photosystem II at 2.9 Å resolution and role of quinones, lipids, channels and chloride. *Nat. Struct. Mol. Biol.* **16,** 334-342 (2009).
6. Kamiya, N. & Shen, J.-R. Crystal structure of oxygen-evolving photosystem II from

Thermosynechococcus vulcanus at 3.7-Å resolution. *Proc. Natl. Acad. Sci. USA* **100**, 98-103 (2003).

7. Kawakami, K., Iwai, M., Ikeuchi, M., Kamiya, N. & Shen, J.-R. Location of PsbY in oxygen-evolving photosystem II revealed by mutagenesis and X-ray crystallography. *FEBS Lett.* **581,** 4983-4987 (2007).
8. Broser, M., Gabdulkhakov, A., Kern, J., Guskov, A., Müh, F., Saenger, W. & Zouni, A. Crystal structure of monomeric photosystem II from *Thermosynechococcus elongatus* at 3.6 Å resolution. *J. Biol. Chem*. **285,** 26255-26262 (2010).
9. De Paula, J. C., Beck, W. F. & Brudvig, G. W. Magnetic properties of manganese in the photosynthetic O_2-evolving complex. 2. Evidence for a manganese tetramer. *J. Am. Chem. Soc*. **108,** 4002-4009 (1986).
10. Carrell, G., Tyryshkin, A. M. Dismukes, G. C. An evaluation of structural models for the photosynthetic water-oxidizing complex derived from spectroscopic and X-ray diffraction signatures. *J. Biol. Inorg. Chem.* **7,** 2-22 (2002).
11. Vincent, J. B. & Christou, G. **A** molecular 'double-pivot' mechanism for water oxidation. *Inorg. Chim. Acta* **136**, L41-43 (1987).
12. Peloquin, J. M. & Britt, R. D. EPR/ENDOR characterization of the physical and electronic structure of the OEC Mn cluster. *Biochim. Biophys. Acta* **1503,** 96-111 (2001).
13. Robblee, J. H., Cince, R. M. & Yachandra, V. K. X-ray spectroscopy-based structure of the Mn cluster and mechanism of photosynthetic oxygen evolution. *Biochim. Biophys. Acta* **1503**, 7-23 (2001).
14. Zein, S. et al. Focusing the view on nature's water-splitting catalyst. *Phil. Trans. R. Soc.* **B 363,** 1167–1177 (2008).
15. Nixon, P. J. & Diner, B. Analysis of water-oxidation mutants constructed in the cyanobacterium *Synechocystis* sp. PCC 6803. *Biochem. Soc. Trans*. **22,** 338-343 (1994).
16. Chu, H.-A., Nguyne, A. P. & Debus, R. J. Amino acid residues that influence the binding of manganese or calcium to Photosystem II. 1. The lumenal inter-helical domains of the D1 polypeptide. *Biochemistry* **34,** 5839-5858 (1995).
17. Hwang, H. J., Dilbeck, P., Debus, R. J. & Burnap, R. L. Mutation of arginine 357 of the CP43 protein of photosystem II severely impairs the catalytic S-state cycle of the H_2O oxidation complex. *Biochemistry* **46,** 11987-11997 (2007).
18. Debus, R. J. Protein ligation of the photosynthetic oxygen-evolving center. *Coord. Chem. Rev*. **252,** 244–258 (2008).
19. Service, R. J., Hillier, W. & Debus, R. J. Evidence from FTIR difference

spectroscopy of an extensive network of hydrogen bonds near the oxygen-evolving Mn_4Ca cluster of Photosystem II involving D1-Glu65, D2-Glu312, and D1-Glu329. *Biochemistry* **49,** 6655–6669 (2010).

20. Murray, J. W. & Barber, J. Structural characteristics of channels and pathways in Photosystem II including the identification of an oxygen channel. *J. Struct. Biol.* **159,** 228–237 (2007).
21. Ho, F. M., & Styring, S. Access channels and methanol binding site to the $CaMn_4$ cluster in Photosystem II based on solvent accessibility simulation, with implications for substrate water access. *Biochim. Biophys. Acta* **1777,** 140–153 (2008).
22. Zhang, C. Low-barrier hydrogen bond plays key role in active photosystem II—A new model for photosynthetic water oxidation. *Biochim. Biophys. Acta* **1767,** 493–499 (2007).
23. Hoganson, C. W. & Babcock, G. T. A metalloradical mechanism for the generation of oxygen from water in photosynthesis. *Science* **277,** 1953-1956 (1997).
24. Tommos, C. & Babcock, G. T. Proton and hydrogen currents in photosynthetic water oxidation. *Biochim. Biophys. Acta* **1458,** 199-219 (2000).
25. Hays, A.-M. A., Vassiliev, I. R., Golbeck, J. H. & Debus, R. J. Role of D1-His190 in the proton-coupled oxidation of tyrosine Y_Z in manganese-depleted Photosystem II. *Biochemistry* **38,** 11851-11865 (1999).
26. Murray, J. W. et al. X-ray crystallography identifies two chloride binding sites in the oxygen evolving centre of Photosystem II. *Energy Environ. Sci.* **1,** 161–166 (2008).
27. Kawakami, K., Umena, Y., Kamiya, N. & Shen, J.-R. Location of chloride and its possible functions in oxygen-evolving Photosystem II revealed by X-ray crystallography. *Proc. Natl. Acad. Sci. U.S.A*. **106,** 8567–8572 (2009).
28. Burrel, J. W. K., Jackman, L. M. & Weedon, B. L. C. Stereochemistry and synthesis of phytol, geraniol, and nerol. *Proc. Chem. Soc.* **1959,** 263-264 (1959).
29. Crabbe, P., Djerassi, C., Eisenbraun, E. J. & Liu, S. Optical rotatory dispersion studies. XXIX. Absolute configuration of phytol. *Proc. Chem. Soc*. **1959,** 264-265 (1959).
30. Vasil'ev, S., Orth, P., Zouni, A., Owens, T. G. & Bruce, D. Excited-state dynamics in photosystem II: Insights from the x-ray crystal structure. *Proc. Natl. Acad. Sci. U.S.A*. **98,** 8602–8607 (2001).
31. Shen, J.-R. & Inoue, Y. Binding and functional properties of two new extrinsic components, cytochrome *c*-550 and a 12 kDa protein, in cyanobacterial

photosystem II. *Biochemistry* **32,** 1825-1832 (1993).
32. Shen, J.-R. & Kamiya, N. Crystallization and the crystal properties of the oxygen-evolving photosystem II from *Synechococcus vulcanus*. *Biochemistry* **39,** 14739-14744 (2000).
33. Yano, J. et al. X-ray damage to the Mn_4Ca complex in single crystals of photosystem II: A case study for metalloprotein crystallography. *Proc. Natl. Acad. Sci. USA* **102**, 12047-12052 (2005).
34. Cruickshank, D. W. J. Remarks about protein structure precision. *Acta Cryst.* **D55,** 583–601 (1999).

Acknowledgements

The X-ray diffraction data was taken at beamlines BL44XU, BL41XU, and BL38B1 of SPring-8. We thank Eiki Yamashita, Nobutaka Shimizu, Seiki Baba, Nobuhiro Mizuno for their help in using the beamlines. JRS thanks Yorinao Inoue for his support in the initiation of this work. This work was supported by a Grant-in-Aid for Scientific Research on Priority Areas (Structures of Biological Macromolecular Assemblies), a Grant-in-Aid for Creative Scientific Research, a GCOE program on Pico-biology at the University of Hyogo, a Grant-in-Aid for Scientific Research (C), from the Ministry of Education, Culture, Sports, Science and Technology of Japan, and a research grant from the Yamada Science foundation.

Author Contributions

KK performed, and JRS supervised the purification and crystallization of PSII. JRS, KK and YU performed X-ray diffraction experiments. YU analyzed the structure, and NK supervised the structure analysis and refinement process. JRS and NK jointly wrote the paper, and all of the authors joined the discussion of the results.

Author Information

Atomic coordinates have been deposited in the Protein Data Bank under the accession number 3ARC. The authors declare no competing financial interests. Correspondence and requests for materials should be addressed to J.R.S. (shen@cc.okayama-u.ac.jp) and N.K. (nkamiya@sci.osaka-cu.ac.jp).

Figure legends

Fig. 1. Overall structure of PSII dimer from *Thermosynechococcus vulcanus* at 1.9 Å resolution. View from the direction perpendicular to the membrane normal. (a) Overall structure. The protein subunits are colored individually in the right-side monomer and in light gray in the left-side monomer, and the cofactors are colored in the left-side monomer and in light gray in the right-side monomer. Orange ball represent water molecules. (b) Arrangement of water molecules in PSII dimer. The protein subunits were expressed in light gray, and all other cofactors were omitted. The central broken lines are the non-crystallographic two-hold axes relating the two monomers.

Fig. 2. Structure of the Mn_4CaO_5-cluster. (a) Determination of individual atoms associated with the Mn_4CaO_5-cluster. Structure of the cluster was superimposed with the 2Fo-Fc map (blue) contoured at 5 σ for Mn and Ca atoms, and omit map (green) contoured at 7 σ for oxygen atoms and water molecules. (b) Distances between metal atoms and oxo-bridges or water molecules (Å). (c) Distances between each pair of Mn atoms. (d) Distances between Mn and the Ca atoms. (e) Stereo view of the Mn_4CaO_5-cluster and its ligand environment. Color codes: Mn, magenta; Ca, yellow; oxygen, red; D1, green; CP43, pink.

Fig. 3. Hydrogen-bond network around Y_Z. (a) Hydrogen-bonds around Y_Z (D1-Tyr161). The bonds between metal atoms and water ligands are depicted as solid lines, and the hydrogen-bonds are depicted as dashed lines. Distances were expressed in Å. (b) Hydrogen-bond network from the Mn_4CaO_5-cluster through Y_Z to the lumenal bulk phase. Water molecules participated in the hydrogen-bond network are depicted in orange, whereas those not participated in the network are in gray. The area painted in green in the upper left side represents the lumenal bulk surface. Color codes: PsbV, pale yellow. Other color codes are the same as in Fig. 2.

Fig. 4. Structure of two Cl^--binding sites. (a) Location of the two Cl^- ions. Blue mesh: 2Fo-Fc map contoured at 4 σ taken at 0.9 Å wavelength; orange mesh: anomalous difference Fourier map contoured at 8 σ taken at 1.75 Å. The small density at the upper left corner was from the S-atom of D1-Met328. Distances were expressed in Å. (b) Hydrogen-bond network from the Mn_4CaO_5-cluster through the Cl-1 binding site to the lumenal bulk phase. (c) Hydrogen-bond network from the Mn_4CaO_5-cluster through the Cl-2 binding site to the lumenal bulk phase. Color codes are the same as in Fig. 2 and 3.

Fig. 5. Organization of chlorophylls. (a) Organization of 35 chlorophylls in a PSII monomer. Chlorophylls whose central Mg are coordinated by water are depicted in orange, and one chlorophyll coordinated by CP43-Asn39 is depicted in blue. All other chlorophylls are coordinated by His and are depicted in green. Trans-membrane helices of D1 and D2 are labeled A-E, and trans-membrane helices of CP47, CP43 are labeled I-VI. (b) Organization of the 4 RC chlorophylls. Mg atoms of chlorophylls are depicted in green, and water molecules in orange. The edge-to-edge distances are depicted at Å. (c) Water ligand and hydrogen-bonds of Chl_{D1}. (d) Water ligand and hydrogen-bonds of Chl_{D2}.

METHODS

Purification and Crystallization

The crystals of dimeric PSII from the thermophilic cyanobacterium *Thermosynechococcus vulcanus* were grown as described previously[6, 32]. In order to improve the crystal quality, the purity and homogeneity of PSII was improved by introducing a re-crystallization step in which, the PSII core complexes were first crystallized within 12-24 hours on ice or at 4^{o}C, and the micro-crystals obtained were collected, re-solubilized, and used for the second crystallization step. Sometimes, the re-crystallization step was repeated to ensure a higher homogeneity of the samples, which were monitored by dynamic light-scattering measurements. The re-crystallization procedure typically decreased the polydispersity of the samples from 30% to around 20%.

The PSII crystals obtained were subjected to a post-crystallization dehydration procedure upon increasing the concentrations of glycerol and PEG in the following way. The crystals were first transferred into a 150 µl buffer solution containing 6 % PEG 3,000 in place of 4-5% PEG 1,450 in the original crystallization buffer concentrations (which contained no glycerol). After 25-30 min incubation at 12°C, half of the buffer volume was replaced with a new buffer containing 1.4 % higher concentration of PEG 3,000 and an additional 2.5% glycerol. This procedure was repeated every 25-30 min until the concentration of glycerol and PEG 3,000 reached 25% and 20%, respectively, in the final buffer. The crystals were then dehydrated against air with a humidity of 75%-90% in the final buffer for 2.5 hours in the incubator at 12°C, and frozen in a flash-cooling nitrogen gas and stored in liquid nitrogen. The crystals thus obtained had an approximate water content of 57%, which is remarkably lower than that of the crystals obtained previously (66%)[32], and also lower than the crystals used to analyze the structure at 2.9 Å resolution (61%)[5]. All of the cryoprotectant replacement and cryo-cooling procedures were carried out under dim green light to avoid possible advancement of the S-states. A typical diffraction pattern of the PSII crystals was shown in Supplementary Fig. 1, from which diffraction spots beyond 1.8 Å resolution could be observed.

Data collection

After dehydration, the crystals were coated with a mixture of oil containing 66.5 % paratone-N, 28.5 % paraffin oil and 5 % glycerol, and flash-cooled at 100 K with a nitrogen gas stream. Two diffraction data sets were collected from two PSII crystals,

one with a wavelength of 0.9 Å and the other one with 1.75 Å, at beamline BL44XU of SPring-8 in Japan. The X-ray beam had a size of 50 x 50 μm^2, and the diffraction images were recorded with a Mar225HE CCD detector. For the data set taken at 0.9 Å wavelength, we used a large PSII crystal of 0.2 x 0.7 x 1.0 mm^3. The crystal was shifted by 30 μm to an adjacent point along the oscillation axis after recording 100 oscillation images, each of which has a 0.2 degree of rotation. Each point therefore covered a range of 20 degrees. We collected a total of 900 images from 9 irradiation points, covering a rotation angle of 180 degrees. The data were processed and scaled using *XDS* and *XSCALE*[35] (Supplementary Table 1).

The photon flux of the beamline used (BL44XU) was 0.7 x 10^{11} photons/sec (with an attenuator of 0.2 mm aluminium), and the exposure time was 1 sec for each diffraction image. This gave rise to a total X-ray dose of 2.5 x 10^{10} photons/μm^2 for the total of 900 images. Since the whole data set was divided into 9 spots on the crystal, each spot received a total dose of 0.28 x 10^{10} photons/μm^2. If we consider that each points were rotated over 20 degrees during the data collection, the X-ray dose irradiated on a unit volume of the crystal will become slightly lower. This dose is much lower than that used previously[3-6], and also in a lower level that was reported to induce possible radiation damage against the Mn_4CaO_5-cluster[33].

For the data set taken at the wavelength of 1.75 Å, we collected 2400 oscillation images, each having a 0.3 degree of rotation over a range of 360 degree. For each of the data wedges of 10 degree, an inverse beam geometry was employed to measure the Friedel's pairs directly. The data was processed with *HKL2000*[36], and the reflection data statistics were summarized in Supplementary Table 1.

Structure refinement

An initial structure of PSII dimer was obtained with the molecular replacement method of *CNS*[37] using the structure of PSII monomer (PDB code: 3BZ1)[5] as a search model. The first stage of structure refinement was carried out using the *CNS* program package and the second stage was performed with *REFMAC5* in the *CCP4* program suite[38]. The two monomers in a PSII dimer were refined separately, and the structural model was revised using *COOT*[39]. Structures of co-factors, lipids, detergents and water molecules were determined and refined as described below. The refinement statistics were presented in Supplementary Table 1.

Mn_4CaO_5-cluster

The locations of the metal atoms, namely, 4 Mn atoms and 1 Ca atom, of the

Mn_4CaO_5-cluster were determined using composite omit 2Fo-Fc map. Oxygen atoms forming oxo-bridges in the Mn_4Ca-cluster were identified and determined with Fo-Fc omit map. The electron density of the O5 atom in the Mn_4CaO_5-cluster was affected heavily by electron density distributions of the nearby metal atoms, which interfered with the determination of its location in the Fo-Fc omit map. Thus, the position of O5 was determined from the 2Fo-Fc map. The average *B*-factor of the 5 metal ions refined without restrain was 25.8 $Å^2$, which was lower than that of the overall average *B*-factor of 35.8 $Å^2$ (Supplementary Table 1).

Chloride and metal ions

The existence of two Cl^- ions in the vicinity of OEC was previously reported with Br^- or I^--substituted PSII[26, 27]. We confirmed the positions of the two Cl^- ion-binding sites in native PSII by both Fo-Fc omit map taken at a wavelength of 0.9 Å analyzed to 1.9 Å resolution, and the anomalous difference Fourier map taken at a wavelength of 1.75 Å analyzed to 2.5 Å resolution. Several additional Ca and Mg ions were identified by these two electron density maps, and their structures were constructed by taking their coordination environments into consideration.

Chlorophyll a and pheophytin molecules

Electron density distributions for the Mg atoms of chlorophyll *a* were clearly separated from those for the chlorin rings and were located out of the ring planes in most cases. The chlorin rings were bended to various degrees depending on their environments. The conformations of ethyl and vinyl groups were determined unambiguously with corresponding electron density distributions. Two optically active centers (C8 and C13) of all of the phytol chains were also recognized as in the *R, R*- configuration from the electron density map.

Plastoquinones

Two plastoquinones, Q_A and Q_B, were identified from the electron density map, whereas the third plastoquinone, Q_C, reported in the previous structure[5] was not observed. Q_A had a well-defined electron density distribution, resulting in a low average *B*-factor of 24.7 $Å^2$, whereas the electron density for Q_B was rather weak, resulting in a higher *B*-factor of 71.6 $Å^2$.

Lipids and unknown molecules

Two kinds of lipid molecules, SQDG and PG, contained sulfur and phosphorous atoms,

respectively, which have larger anomalous dispersion effects at a longer wavelength. The positions of 4 out of 8 SQDG and 8 out of 10 PG molecules in a PSII dimer were confirmed from the anomalous dispersion of the sulfur and phosphate atoms contained in these lipids, based on the anomalous difference Fourier map calculated from the data set taken at 1.75 Å wavelength. The electron densities for a typical SQDG and PG were depicted in Supplementary Fig. 2. Other lipid molecules were found and modeled based on the Fo-Fc omit map and 2Fo-Fc map. Six lipids with two fatty acid chains were found in a dimer, whose species could not be identified. Additionally, 30 single alkyl chains with unknown identity were observed in a dimer, among which, 23 chains were located adjacently. Therefore, the total number of lipids should exceed 23 in a monomer.

Water molecules

Water molecules were assigned from the 2Fo-Fc electron density map over 1 σ level. Around 1300 water molecules were found in a monomer (Supplementary Table 1), a few of them were found to be disordered.

Error estimation for atomic coordinates

The coordinate error was estimated with the diffraction-component precision index (DPI) introduced by Cruikshank[34, 40], with the software *SFCHECK* in *CCP4* suit[38]. The DPI value of whole PSII structure obtained was 0.11 Å, resulting in a standard uncertainty of the bond length of 0.16 Å.

35. Kabsch, W. Automatic processing of rotation diffraction data from crystals of initially unknown symmetry and cell constants. *J. Appl. Cryst.* **26**, 795-800 (1993).
36. Otwinowski, Z. & Minor, M. Processing of X-ray diffraction data collected in oscillation mode. *Methods in Enzymology* **276 part A,** 307-326 (1997).
37. Brünger, A. T. et al. Crystallography & NMR system: A new software suite for macromolecular structure determination. *Acta Cryst.* **D54,** 905-921 (1998).
38. Collaborative Computational Project, No 4 The *CCP*4 suite: programs for protein crystallography. *Acta. Cryst.* **D50,** 760-763 (1994).
39. Emsley, P., Lohkamp, B., Scott, W. G. & Cowtan, K. Features and development of Coot. *Acta Cryst*. **D66,** 486-501 (2010)
40. Daopin, S., Davies, D. R., Schlunegger, M. P. & Grütter, M. G. Comparison of two crystal structures of TGF-*β*2: the accuracy of refined protein structures. *Acta Cryst*. **D50,** 85-92 (1994).

Fig. 1

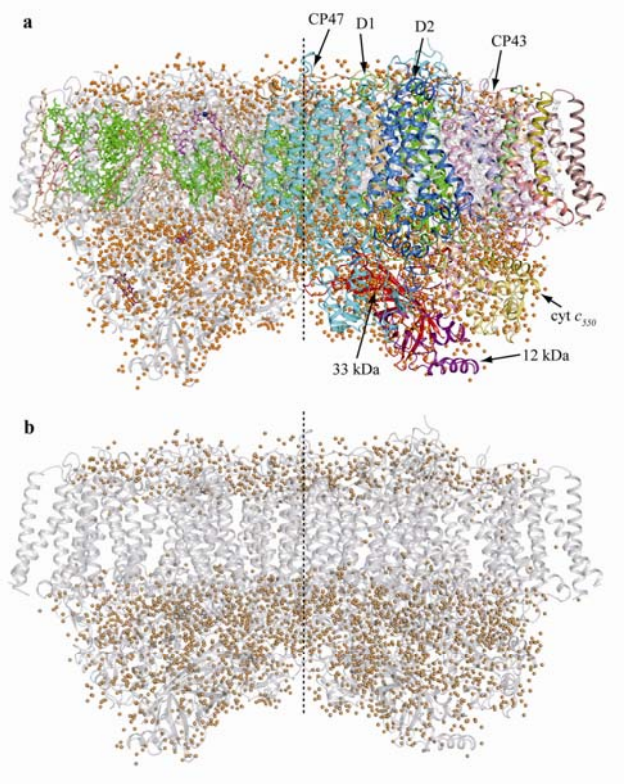

Fig. 2

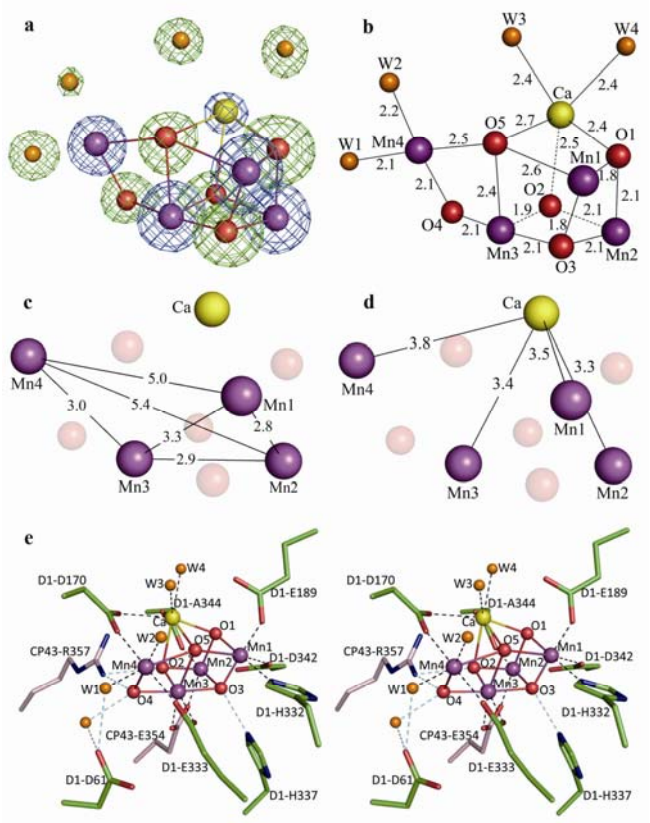
a
b
W3
W4
W2
Ca
2.4
2.4
2.2
O5
2.7
2.4
O1
W1
Mn4
2.5
2.5
Mn1
2.1
2.6
1.8
2.1
2.1
2.4
O2
1.9
2.1
O4
2.1
1.8
Mn3
2.1
2.1
Mn2
O3
c
Ca
Mn4
5.0
3.0
5.4
Mn1
2.8
3.3
2.9
Mn3
Mn2
d
Ca
3.8
3.5
3.3
Mn4
3.4
Mn1
Mn3
Mn2
e
D1-D170
W4
W3
D1-A344
D1-E189
Ca
O1
W2
O5
Mn1
CP43-R357
Mn4
O2
Mn2
D1-D342
Mn3
W1
O4
O3
D1-H332
CP43-E354
D1-E333
D1-D61
D1-H337

Fig. 3

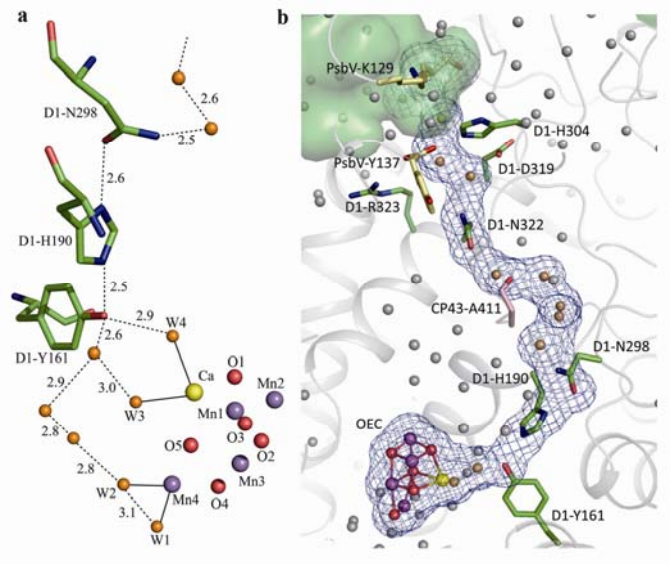
a
D1-N298
2.6
2.5
2.6
D1-H190
2.5
2.9
W4
2.6
D1-Y161
Ca
O1
Mn2
2.9
3.0
W3
Mn1
2.8
O5
O3
O2
2.8
Mn3
W2
Mn4
O4
3.1
W1
b
PsbV-K129
D1-H304
PsbV-Y137
D1-D319
D1-R323
D1-N322
CP43-A411
D1-N298
D1-H190
OEC
D1-Y161

Fig. 4

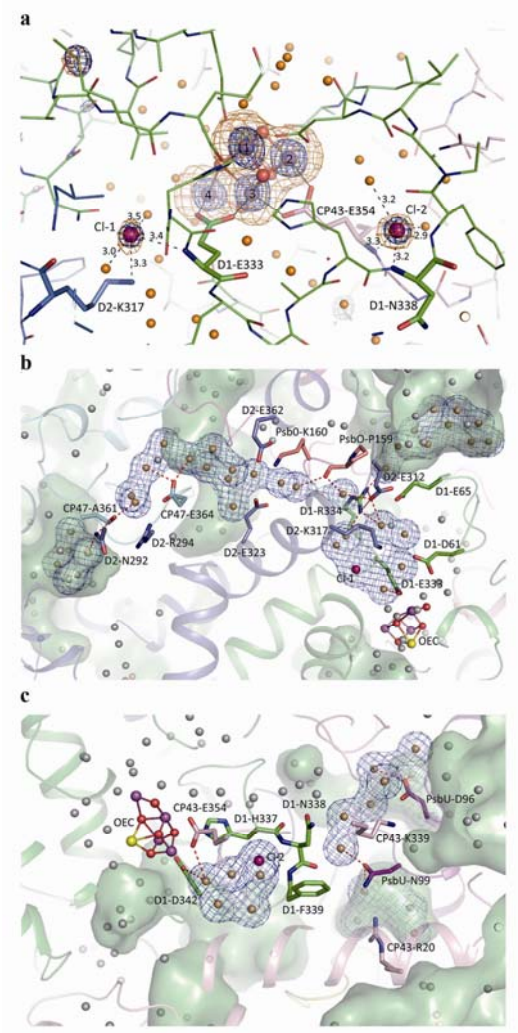
a
Cl-1
Cl-2
CP43-E354
D1-E333
D2-K317
D1-N338
b
D2-E362
PsbO-K160
PsbO-P159
D2-E312
D1-E65
CP47-A361
CP47-E364
D1-R334
D2-K317
D2-R294
D2-E323
D2-N292
D1-D61
Cl-1
D1-E339
OEC
c
CP43-E354
D1-N338
PsbU-D96
OEC
D1-H337
CP43-K339
Cl-2
PsbU-N99
D1-D342
D1-F339
CP43-R20

Fig. 5

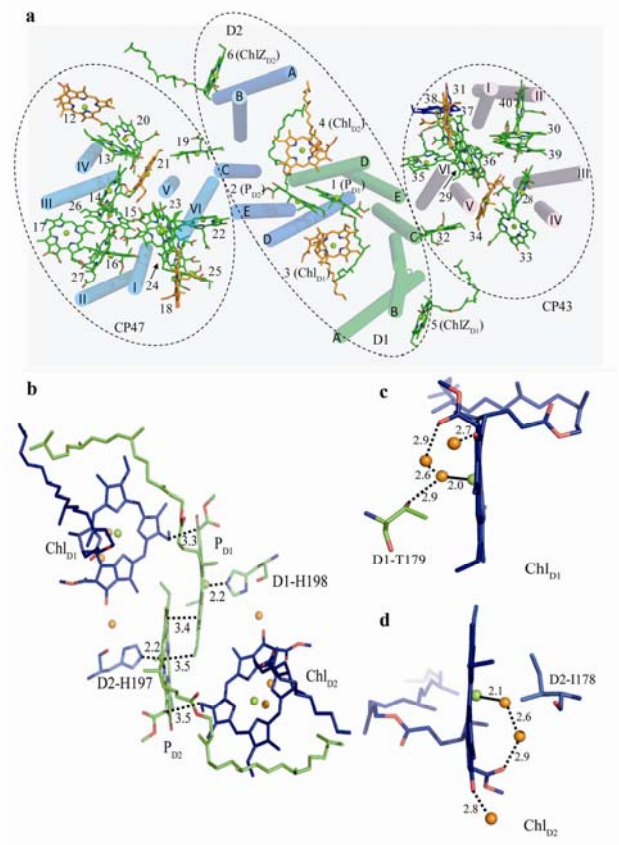
a
D2
6 (ChlZ$_{D2}$)
4 (Chl$_{D2}$)
1 (P$_{D1}$)
2 (P$_{D2}$)
3 (Chl$_{D1}$)
5 (ChlZ$_{D1}$)
CP47
CP43
D1
b
Chl$_{D1}$
P$_{D1}$
D1-H198
D2-H197
Chl$_{D2}$
P$_{D2}$
c
D1-T179
Chl$_{D1}$
d
D2-I178
Chl$_{D2}$